Superhydrophilic and underwater superoleophobic Ti foam with robust nanoarray structures of TiO$_2$ for effective oil-in-water emulsion separation

Luhong Zhang, Xiaodong Yang, Bin Jiang, Yongli Sun, Ziqiang Gong, Na Zhang, Shuai Hou, Jingshuai Li, Na Yang[*]

School of Chemical Engineering and Technology, Tianjin University, Tianjin 300072, China

A B S T R A C T

In this work, a superhydrophilic and underwater superoleophobic Ti foam with TiO$_2$ nanoarrays was facilely fabricated via the hydrothermal treatment and proton exchange method. Taking advantages of the constructed hierarchical structures and the high surface energy of TiO$_2$, the Ti foam exhibits excellent superwetting behaviors to water and ultralow oil adhesion property with the underwater oil contact angle (OCA) of 166° and the sliding angle (OSA) lower than 3°. Meanwhile, the as-prepared foam can be applied for separating various oil-in-water emulsions with 99% separation efficiency and high permeation fluxes. Additionally, it performed good anti-fouling and self-cleaning property, which had stable separation performance even for 50 cycles of repeated use. Importantly, the hierarchical structured sample showed outstanding chemical stability and robust mechanical durability under various chemical corrosions, physical abrasion and vibration without obvious reduction of the separation efficiency. It is expected that superhydrophilic Ti foam with nanoarray structures constructed by this facile method would be a practical candidate in oily wastewater purification, due to its excellent wetting property, good self-cleaning capacity, robust mechanical durability, as well as superior chemical stability.

1. Introduction

Oil pollution by industrial oily sewage discharge and accidental marine oil spills has occurred increasingly catastrophic consequences for water environment and ecology system [1–3]. Generally, oil-contaminated water contains poisonous compounds such as polycyclic aromatic hydrocarbons (PAHs) [4,5]. Therefore, it is essential to effectively separate oil from oily wastewater for water resource protection and oil collection. The conventional techniques including skimming [6], flotation [7], centrifugation [8], in-situ burning [9] and demulsification [10] have been proposed to accomplish the purification of oily wastewater. However, most of these methods are limited by the low separation efficiency, high energy waste, long-term treatment, and secondary pollution.

Inspired by lotus leaf [11,12], the separation of oil/water mixtures can be realized through the superhydrophobic/superoleophilic property of materials. Sponge [13], polymeric membrane [14], metal mesh [15], and natural fibers [16], etc. are modified into superhydrophobic/ superoleophilic materials by multifarious disposal techniques, such as chemical vapor deposition [17], electrospinning [18], electrochemical

etching [19], surface grafting [20] and 3D printing [21], etc. Nevertheless, owing to the intrinsic oleophilicity of these oil-removal materials, they are easily contaminated and clogged by the absorbed oil [22]. Apart from the above "oil-removing" type, the superhydrophilic/ underwater superoleophobic materials inspired by fish scale [23,24] with low adhesion of oil in oil/water/solid three phase system provided a feasible and alternative approach for overcoming these drawbacks and removing water from oil in recent years. This "water-removing" material could generate repulsive force to oil and prevent the surface from being contaminated, which can be recycled in repeated separation process. In addition, since the density of the water is higher than most oily species, the water can pass through the materials driven by the gravity only which is appropriate for the large-scale purification of oily water. Thus, many researches have been reported to construct the superhydrophilic and underwater superoleophobic surfaces [25]. However, these approaches mostly made use of the organic polymer [26], for example, the inorganic matrix covered with the polymeric coatings [27], and the polymer coated with inorganic nanoparticles [28], which frequently need tedious preparation process as well as suffer from the weakness of bad stability, weak environment adaptability, and poor

mechanical stability. Therefore, it is highly demanded to fabricate materials with robust structures adapting to severe environments through a facile method for long-term oil/water separation. Nowadays, the completely inorganic materials with good environment adaptability, mechanical stability, and chemical stability have become an increasingly active topic [29].

TiO$_2$ is considered to be environmentally friendly, chemically stable, intrinsically hydrophilic, which has long been intensively studied for broadening applications in lithium storage [30], photocatalysis [31], oil/water separation [32], etc. However, most of TiO$_2$ nanomaterials employed in separating oil/water mixtures are nanoparticles that incorporate with other substrates, such as polymer membrane [33], stainless metal [34], and fabric [35]. This unstable combination easily leads to the destruction of microstructure under physical or chemical actions, like impact, abrasion, extrusion and corrosion. Fortunately, TiO$_2$ nanomaterials immobilized on the substrates can avoid the falling of nanoparticles and reduce the secondary pollution [36]. Different nanostructures of TiO$_2$, such as nanotubes, nanowires, nanobelts, and nanosheets, are fabricated by various synthesis methods. Among these approaches, the layered titanates which alkali metal cooperated with pure Ti induces have emerged as a facile technique to obtain TiO$_2$ hierarchical nanostructures. The Ti substrate not only provides a Ti source to form the nanostructures, but acts as a plate to support direct growth of nanoarrays. It's known that the materials with superhydrophilic and underwater superoleophobic property can be fabricated through introducing the composition of high surface energy, and constructing micro/nano-surface structures for the roughness [37]. Moreover, to separate the oil/water emulsions, one efficient strategy is using the superhydrophilic materials with a pore size much smaller than the emulsified oil droplets [38]. Therefore, we envisage that porous Ti foam with the appropriate accuracy can realize the separation purpose if hierarchical TiO$_2$ nanoarray structures are integrated with it.

Herein, highly oriented TiO$_2$ nanoarrays were constructed on Ti foam through a facile one-step hydrothermal treatment, followed by the proton exchange and calcination to separate oil-in-water emulsion (Scheme 1). The as-prepared surface with well-designed nanoarray structures showed superhydrophilic and underwater superoleophobic properties. Moreover, the tightly immobilized TiO$_2$ nanoarrays exhibited ultralow oil adhesion and self-cleaning performance, which had stable separation performance even for 50 cycles of repeated use. Importantly, the Ti foam could still maintain its high separation efficiency under different harsh environments of strongly acidic, alkaline, saline solution, organic solvent, performing excellent anti-corrosion ability. In addition, the nanoarray crystals which stably grew on the Ti substrate could avoid the easy destruction from the impact of physical abrasion

and vibration. Hence, our research shows that the modified Ti-based materials with controllable TiO$_2$ nanoarray structures through a facile method can both overcome the weakness of tedious fabrication process, easy fouling, and adapt different environments when separating oily water. The fabrication of superhydrophilic Ti foam provides a practical candidate for efficient oil-in-water emulsion separation and water remediation under a series of severe conditions.

2. Experimental

2.1. Materials

All reagents were of analytical grade and used without further purification. Ti foam (purity ≥ 99%, size 30 × 30 mm^2, thickness 1 mm, accuracy 5 μm) was purchased from Teng Erhui Electronic Technology Co., Ltd. (Kunshan, China). Acetone (analytical purity) and isopropanol (analytical purity) were obtained from Jiangtian Chemical Technology Co., Ltd. (Tianjin, China). Sodium hydroxide (NaOH, guaranteed purity) was purchased from Tianjin Komeo Chemical Reagent Co., Ltd. Hydrochloric acid (HCl, 37 wt%) were supplied by Real & lead Reagent Co., Ltd. (Tianjin, China). Deionized water was used in all experiments.

2.2. Fabrication of superhydrophilic Ti foam

Ti foams with a size of 30 × 30 × 1 mm^3 were cleaned sequentially by ultrasonic washing in acetone, isopropanol, and distillation water for 10 min to remove the surface impurities thoroughly. The fabrication process was based on the previous report with some modifications [39]. The post-ultrasonic Ti foams were transferred to an 80 ml Teflon-lined stainless-steel autoclave filled with 60 ml 2 M NaOH solution. The autoclave was heated at 160 °C for different time (1–16 h), and then air-cooled to room temperature. After the hydrothermal treatment, the modified Ti foams were washed with deionized water for several times, then immersed into 0.1 M HCl for 1 h. Subsequently, it was taken out and dried at 60 °C in an oven. Last, the as-prepared samples were obtained after calcination at 450 °C for 2 h.

2.3. Surface characterization

The surface morphologies of the as-treated Ti foams with different hydrothermal time at 160 °C were characterized by scanning the electron microscopy (SEM, S-4800, Hitachi, Japan) with 5 kV accelerating voltage and 10 μA current. XRD (D8-Focus, AXS, Germany) data was examined at the 2θ range of 5–80° and scanning rate of 8°/min by using
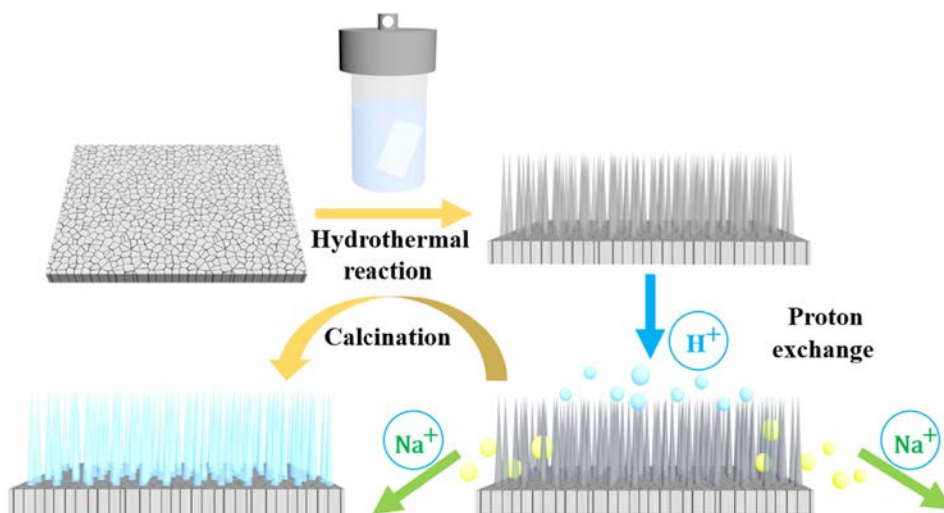
Scheme 1. Scheme illustration of synthesis process of superhydrophilic Ti foam with nanoarray structures.
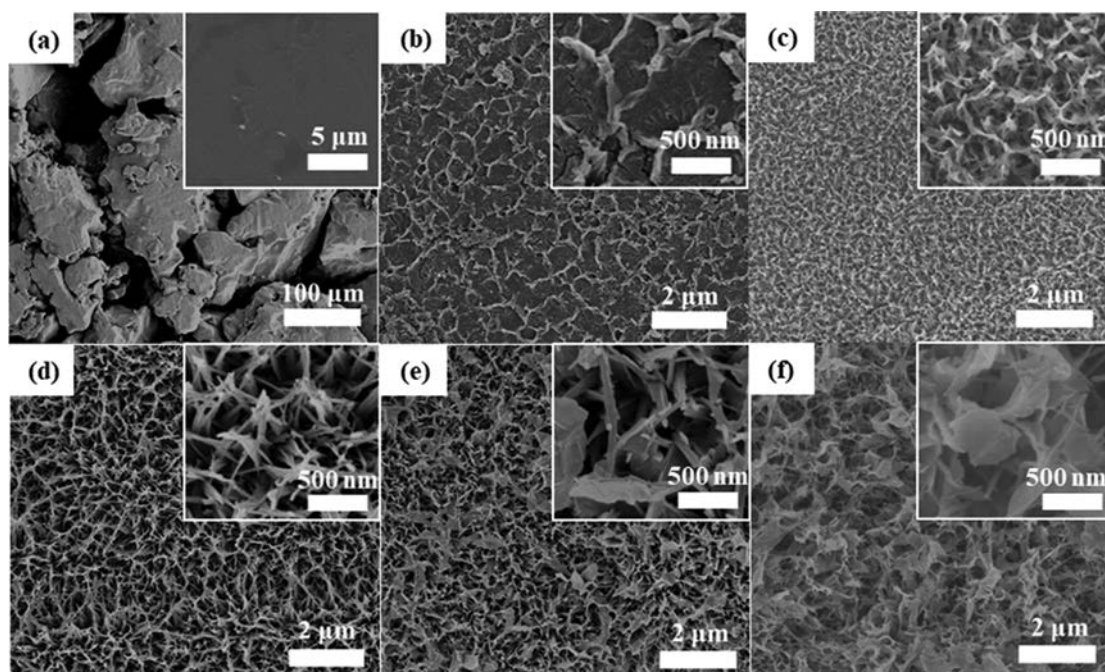
Fig. 1. SEM images of Ti foam surfaces for different hydrothermal time (a) 0 h, (b) 1 h, (c) 2 h, (d) 3 h, (e) 6 h, (f) 10 h. The insets were corresponding high magnification images.

Cu Kα (λ = 1.54056 Å) radiation to evaluate the external crystalline structure. The X-ray photoelectron spectroscopy (XPS, Thermo ESCALAB 250Xi, USA) was performed to analyze the surface composition.

The water contact angle was measured by dropping water droplet on the surface of the sample and the diffusion process was recorded by a high-speed camera. The as-prepared Ti foam was immobilized on the plate. The underwater oil contact angle (OCA) and oil sliding angle (OSA) were measured with 5–8 μL of oil droplet dropping on the surface of the as-prepared Ti foam in water by using an optical contact angle and an interface tension meter (SL200KS, KINO, USA) at ambient temperature. For the light oil, we firstly fixed and adjusted the plate in a transparent cube pot containing water, then injected different oils from the upward side of water by using the specially crooked needle onto the downside of the samples. The OCAs and OSAs were obtained by averaging the values of the sample at five different positions.

2.4. Oil/water separation experiment

The as-prepared Ti foams were fixed between two glass tubes in 20 mm diameter connected with two stainless steel flanges. The entirety was fastened via nuts and bolts to form a filtration apparatus. All the separation processes were achieved by gravity. Various kinds of oils including diesel, petroleum ether, n-hexane, kerosene, toluene and soybean oil were used to prepare oil-in-water emulsion. There were two steps of preparation for oil-in-water emulsion. First, add 10 g oil into 1000 ml distillation water in plastic measuring cup, and then sharply stir by operating a homogenizer (Fluke homogenizer, FA25, 500 W) at 12,000 rpm for 3 min.

The oil/water emulsion was separated through aforementioned apparatus, and water in the filtrate was collected in a beaker, then oil in the filtrated water was extracted by CCl₄. Here, an infrared oil content analyzer (F2000, China) was adopted to measure the content of filtrated oil. The oil content of each sample was the average value from five measurements. The oil/water separation efficiency was defined by the oil rejection coefficient η (%) using the following Eq. (1) and the permeation flux F of the as-prepared Ti foam was calculated by following Eq. (2):

$$\eta = \left(1 - \frac{C_P}{C_0}\right) \times 100\% \tag{1}$$

$$F = \frac{V}{A \times t} \tag{2}$$

For Eq. (1), where C_P and C_0 represent the post-filtration oil concentration and the original oil/water emulsion, respectively. For Eq. (2), where V represents the volume of permeation, A is the effective filtration area of the as-prepared Ti foam and t stands for the filtration time.

2.5. Anti-fouling and self-cleaning performance

The samples (pristine and as-prepared foam) pre-wetted with water were contaminated by machine oil (labeled by oil red) and immersed in water. Then, the oil droplet was injected onto the surface of as-prepared Ti foam underwater for the test by a syringe. Eventually, the samples were immersed in oily sewage for several times for further exploring the self-cleaning performance.

2.6. Corrosion resistance test

The as-prepared Ti foam was immersed in the corrosive solutions of 1 mol L⁻¹ HCl, 1 mol L⁻¹ NaOH, 1 mol L⁻¹ NaCl, hot water (80 °C), ice water (0 °C) and various organic solvents (acetone, toluene, chloroform, isooctane, ethyl acetate) for 24 h, respectively. Then, the underwater OCA and the separation efficiency were measured to evaluate the anti-corrosive property and chemical stability.

2.7. Mechanical strength tests

The ultrasonic vibration and abrasion treatment were used to test the mechanical stability. The as-prepared Ti foam was vibrated by an ultrasonic cleaner (KQ-22, Yuhua Instrument, China) with different time, then the underwater OCAs and OSAs were recorded to assess the wetting behaviors. The abrasion test was conducted on a sandpaper of 400 mesh for pulling forward and back. After certain cycles, the separation efficiencies of the rubbed Ti foam were calculated to evaluate

the mechanical strength.

3. Results and discussion

3.1. Characterization and surface morphology of fabricated Ti foam

The Ti foam composed of irregular particles is rich in foam pores which are created by pressing, forming, and removing of pore forming agent (Fig. S1). As shown in Fig. 1, the surface morphologies of Ti foam with various hydrothermal reaction time (0–10 h) were investigated by SEM. Particularly, the invariable reaction temperature was set at 160 °C and the concentration of NaOH aqueous was 2 M. The SEM imaging showed the evolution of surface morphology from the initial humps, to nanobelts, nanowires until final thick sheets. It was worth noting that the surface of pristine Ti foam was relatively smooth at higher magnification as shown in Fig. 1a. The surface of the Ti foam became rough due to the hydrothermal reaction, resulting in the obvious nano/micro scale arrays. With a short duration of hydrothermal treatment (1 h), the rough and wrinkled humps which provided growth sites for the nanobelts in the next stage appeared on the surface. (Fig. 1b). By increasing the hydrothermal time to 2 h (Fig. 1c), numerous curly nanobelts with a preferentially vertical orientation came out. Then, the hierarchical nanowires structure formed when the reaction time was extended to 3 h (Fig. 1d). When the hydrothermal time continued to increase (6,10 h), thick sheets came into being and grew as illustrated in Fig. 1e-f. Combining the roughness based on the surface morphology with the hydrophilicity, it is appropriate to determine that the sample with reaction time of 3 h owned optimal superhydrophilicity because of its dense and uniform nanoarray. Moreover, underwater OCAs of foam samples with various hydrothermal time were applied to further investigate their wettability by dropping dichloromethane on surfaces. As illustrated in Fig. 2, the underwater OCA of pristine Ti foam was 132° and it increased to 153° after the hydrothermal treatment of 1 h. When the reaction time was prolonged to 2 h, 3 h, 4 h (Fig. S2), the underwater OCAs exceeded 160°, exhibiting the improvement of underwater superoleophobic performance. However, owing to the reduction of surface roughness, the underwater OCA decreased below 158° when the hydrothermal time was more than 6 h. Consequently, the hydrothermal time of 3 h was chosen as the optimal value, and the corresponding synthesized materials were used to evaluate the surface wettability and separation ability.

The superhydrophilic property was ascribed to the combination of the hierarchical nanoarray structures and the high surface energy assembled on the Ti foam. To confirm the composition of this hierarchical nanowires, the surface of Ti foam was measured by XRD and XPS.
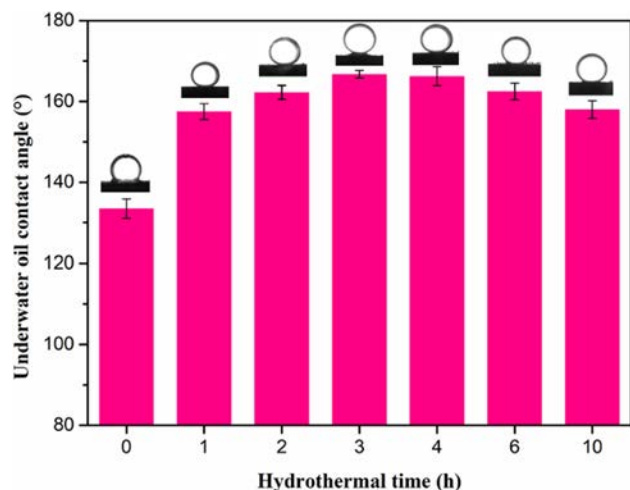

Fig. 2. Underwater OCAs of the as-prepared Ti foam with different hydrothermal time.

Fig. 3a showed the XRD spectrum of hydrothermal Ti foam. The 2θ peaks at 25.4°, and 48.2° correspond to the anatase facets of (1 0 1), (2 0 0), respectively, in agreement with the standard TiO$_2$ anatase cards (JCPDS card no.21–1272), which confirmed the formation of TiO$_2$ [40]. XPS was further employed to investigate the surface components and chemical states. Fig. 3b shows the XPS survey spectra of as-prepared superhydrophilic foam. The existence of Ti, O, C in the as-prepared Ti foam sample confirmed the successful introduction of O atoms after the hydrothermal treatment. Sharp photoelectron peaks locating at binding energy at 459, 530, and 486 eV belonged to Ti 2p, O 1s, and C 1s, respectively, in which the C peaks was attributed to absorbed carbon specimen. The high-resolution pattern of Ti 2p for the foam sample was shown in Fig. 3c. Two peaks at 458.5 and 464.2 eV were related to the Ti 2p$_{3/2}$ and Ti 2p$_{1/2}$, respectively, which confirmed the existence of Ti^{4+} in TiO$_2$ [41]. The O 1s spectra was split into two symmetrical peaks at 529.7 eV and 531.1 eV (Fig. 3d), which were in agreement with the binding energy of the Ti-O bond [42] and the surface Ti-OH species [43], respectively. The results of XRD and XPS both indicated the formation of TiO$_2$.

3.2. Formation mechanism of the TiO$_2$ nanostructures

Based on the above characterization results and previous studies, the formation mechanism of TiO$_2$ nanoarray structures are as follows [44].

$$2Ti + 2NaOH + 3H_2 O \rightarrow Na_2Ti_2O_5 \cdot H_2 O + 4H_2 \tag{1}$$

$$Na_2Ti_2O_5 \cdot H_2 O + 2HCl \rightarrow H_2Ti_2O_5 \cdot H_2 O + 2NaCl \tag{2}$$

$$H_2Ti_2O_5 \cdot H_2 O \rightarrow 2TiO_2 + 2H_2O \tag{3}$$
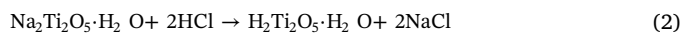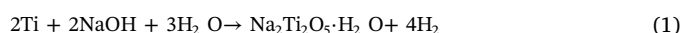
The Ti foam acted as both the Ti source and the substrate. In the beginning, NaOH aqueous solution reacted with Ti substrate to generate Na$_2$Ti$_2$O$_5$·H$_2$O nanocrystalline covering the surface of foam. The Na$_2$Ti$_2$O$_5$·H$_2$O nanocrystalline acting as nuclei (Fig. 4a) began to grow into nanobelts (Fig. 4b) with the hydrothermal treatment. The growth of the cross direction to the substrate was limited due to the intense growth competition in numerous nucleation sites simultaneously, whereas the growth in the vertical direction was free. Therefore, with the Ti atoms inside of foam diffusing to the surface to supply Ti source, the nanobelts continued to grow in the perpendicular direction to the substrate. However, the TiO$_2$ nanobelts elongated but also shrank as the reaction time is prolonged [45]. When the nanobelts grew, the defect strain caused by the dislocations in the cross direction was increasing. Interestingly, the growing defect strain with nanobelts growth conversely suppressed the nanobelts into nanowires, as shown in Fig. 4c. The whole formation progress could be explained as "nucleation-dissolution–recrystallization". Meanwhile, because of the possible reaction taking place between Ti and Na$_2$Ti$_2$O$_5$·H$_2$O dissolving to the solution, thick sheets were formed [46]. Thicker sheets aggregated randomly in all directions when Na$_2$Ti$_2$O$_5$·H$_2$O recrystallized on the surfaces of the former metastable sheets (Fig. 4d). With the prolongation of reaction time, more and more thicker sheets and slenderer nanowires appeared simultaneously for the difficulty diffusion of NaOH as shown in Fig. 4e. Nevertheless, disorder sheets and nanowires distributed irregularly on the surface, where nanowires leaned against thick sheets and became web-like in Fig. 4f. The corresponding cross-section images of the samples for different hydrothermal time are shown in Fig. S3 to further show the revolution of surface morphologies. The different samples show various surface morphologies from curly nanobelts (2 h), nanowires (3 h), nanowires/nanosheets (4 h), to thick sheets (6 h), web-like wires/thick sheets (10 h). Here, combining the SEM results with the previous studies, we deduced that there are two main factors described above sequentially influencing the surface morphology, including the defect strain and Na$_2$Ti$_2$O$_5$·H$_2$O recrystallization. The former dominated the formation of nanowires, while the latter promoted the growth of nanobelts as well as the thick sheets. The formation process based on
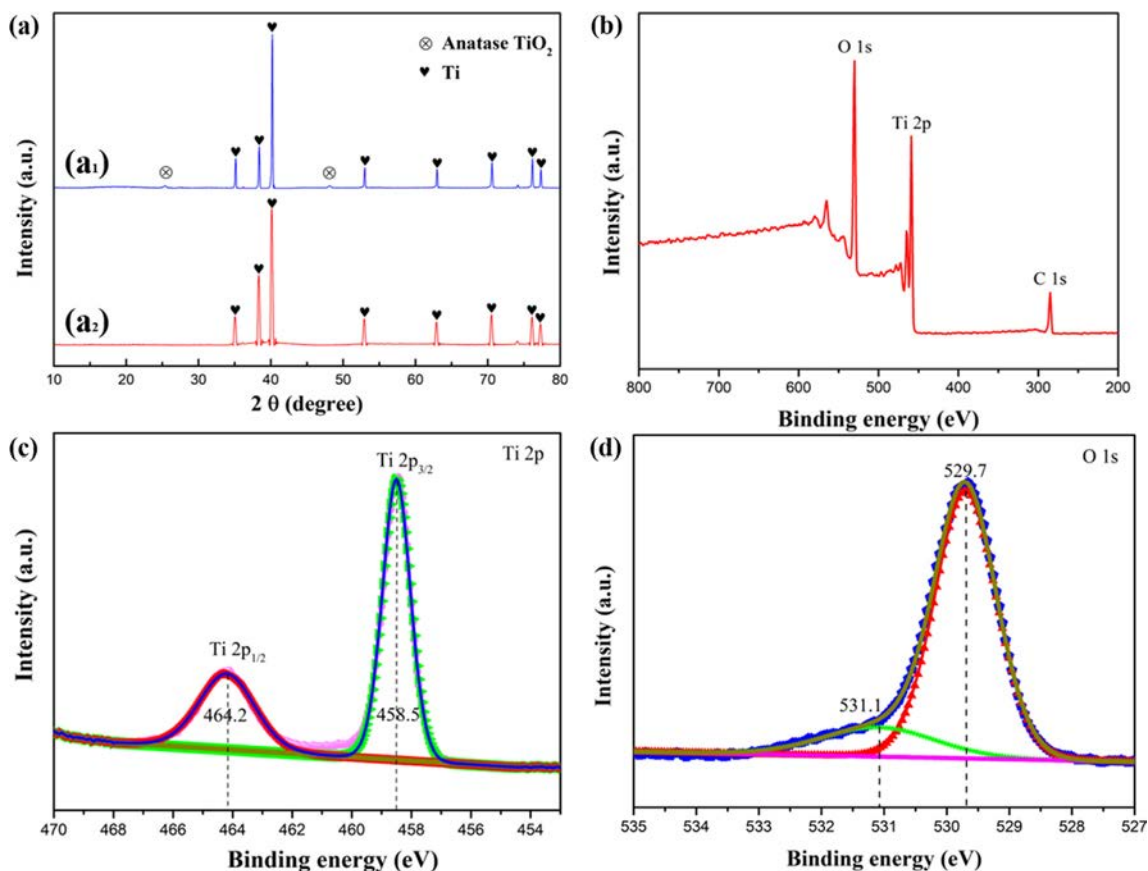
Fig. 3. (a) XRD patterns of (a_1) pristine Ti foam, (a_2) superhydrophilic Ti foam and XPS spectra of (b) full spectrum, (c, d) high-resolution of Ti 2p and O1s peak fitting, respectively.

the aforementioned results could be expressed into three steps: (i) nucleation and formation of nanobelts, (ii) formation and growth of nanowires; (ii) appearance and growth of thick sheets. Eventually, sheets were gradually dissolved because of the alkaline environment when the reaction reached to 16 h, which caused the disappearance of nanostructures as shown in Fig. S4.

The as-prepared Ti foams with different hydrothermal reaction time showing diverse nano/micro structures were immersed into HCl aqueous solution for 1 h to realize ion exchange from Na^+ to H^+. The $H_2Ti_2O_5·H_2O$ was formed by this method. The resulting hydrogen titanate was annealed to dehydrate and eventually converted to anatase TiO_2 at 450 °C for 2 h. The whole progress of acid leaching and calcination still maintained the complete structure, and never changed the morphology [47]. The synergistic effect of the nanoarray surface's
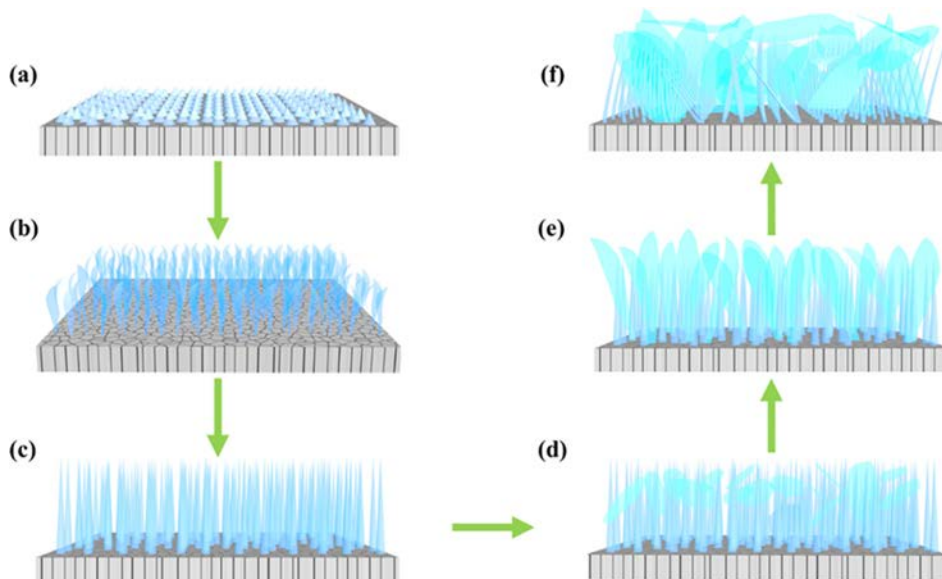

Fig. 4. Formation and growth process of TiO_2 nanoarray and thick sheets.
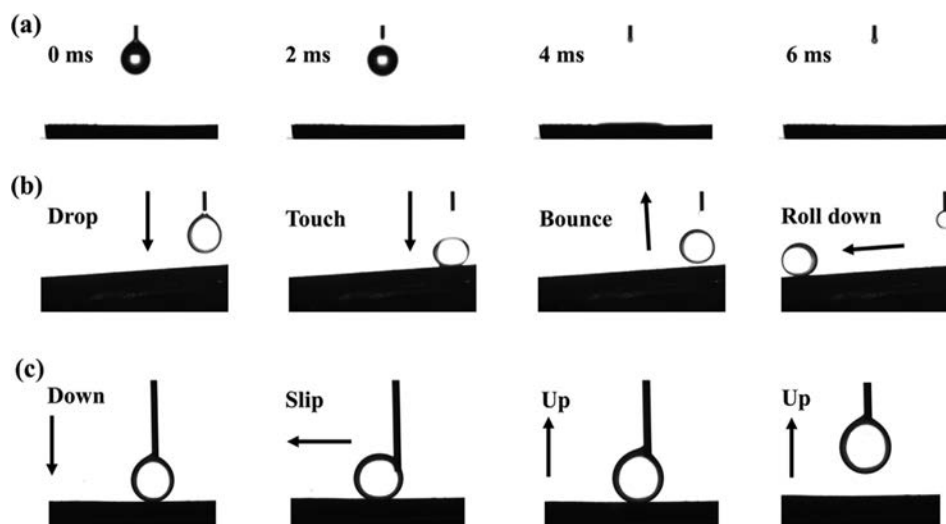
Fig. 5. Dynamic pictures of water droplet on the surface. (a) The rapid water wetting process and (b) several oils droplets rolled down with the superhydrophilic Ti foam. (c) Low adhesion test between the oil droplet and the surface underwater.

roughness and high surface energy of TiO_2 resulted in superhydrophilic surfaces. Comparing with underwater superoleophobic materials that separate oil-in-water emulsions by gravity driven (Table 1 in Supplementary material), the fabrication process of our samples displays facile and manageable characteristic.

3.3. Wettability of the foam

As is well known, the wetting behavior of solid surfaces was determined by the geometrical structure and chemical composition [37]. The establishment for vertical growth of nanoarray TiO_2 contributed to realize the superhydrophilicity. For the pristine porous Ti foam, the lack of the rough structures made the water droplet remain on the surface with the high WCA of 122° in air (see Fig. S5). However, owing to high surface energy of TiO_2 and nanoscale rough structures covering the as-prepared Ti foam, the water droplet spread out instantly when dropped on sample's surface (Video S1), exhibiting excellent superhydrophilic property. It could be observed that WCA is obviously 0° in Fig. 5a, showing the rapid wetting process in 4 ms. Compared with the phenomenon in air, the wettability to oil was greatly altered when the Ti foam were immersed in water. Moreover, we measured the underwater OCAs and OSAs as shown in Fig. 6. The results of contact angle

Fig. 6. Underwater OCAs and OSAs of different oils on the superhydrophilic Ti foam.

test of diesel, n-hexane, kerosene, soybean oil, petroleum ether and dichloromethane with OCA larger than 160° and the OSA less than 3° exhibited outstanding underwater superoleophobicity and oil-repellent property for the as-prepared Ti foam. This phenomenon is attributed to the water molecules being trapped in the micro/nanostructures, which prevents the oil phase permeating into the solid surface, forming a "Cassie–Baxter" state at the composite oil/water/solid interface [48].

The dynamic adhesion test was utilized to investigate the underwater oil-repellent abilities of the Ti foam, including underwater oil sliding process in a tilting angle of 3° as well as oil droplet pressing-lifting experiment. As shown in Fig. 5b, a high-speed camera system recorded the adhesion process of oil droplet dropping on the Ti foam. When injected on the surface, the droplets bounced immediately, dropped and rolled down along with the surface by gravity. Additionally, as shown in Fig. 5c, the adhesion test was further performed on a flat as-prepared Ti foam by a needle. The oil drop squeezed out of shape slipped away for a short distance under pressure but followed the needle away from the surface without any adhesion. The above results demonstrated that the superhydrophilic Ti foam possessed underwater superoleophobicity and ultralow oil adhesion.

3.4. Oil/water emulsions separation

A series of oil-in-water emulsions with micron sized droplets were prepared to evaluate the separation capability of the as-prepared Ti foam. As shown in Fig. 7, the simple filtration device was only driven by gravity without any external pressure. It consisted of two straight glass tubes stuffed by sample foam and fixed flanges, a beaker for collecting the separated water. Before separation, the as-prepared Ti foam was wetted by water. When the milky emulsion touched the wetted foam, continuous and transparent water phase immediately penetrated through the foam and flow down into the beaker, while oil droplets were intercepted on the upper tube (Video S2). Fig. 8 showed the optical microscope images of the emulsion (kerosene) before and after separation. No small oil droplets were found in the collected filtrate compared with that obvious droplets in the emulsions, implying that the oil had been successfully removed. The sizes of some emulsified oil droplets reached 4 μm or below, while the pore size of Ti foam (accuracy 5 μm) composed of irregular tiny Ti particles is hard to confirm, and reduced after hydrothermal reaction due to the extension of plenty of nanoarrays. (Fig. S6). The strong affinity of TiO_2 toward water molecules can form a surface-adsorbed water layer, which make sure dispersed oil droplets do not contact with the wetting surface [49]. The
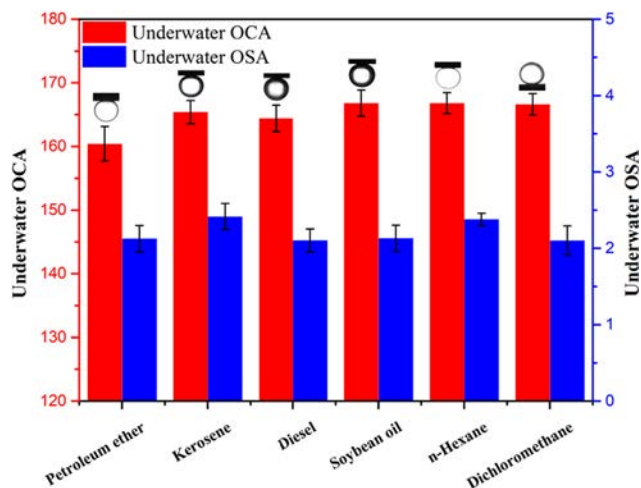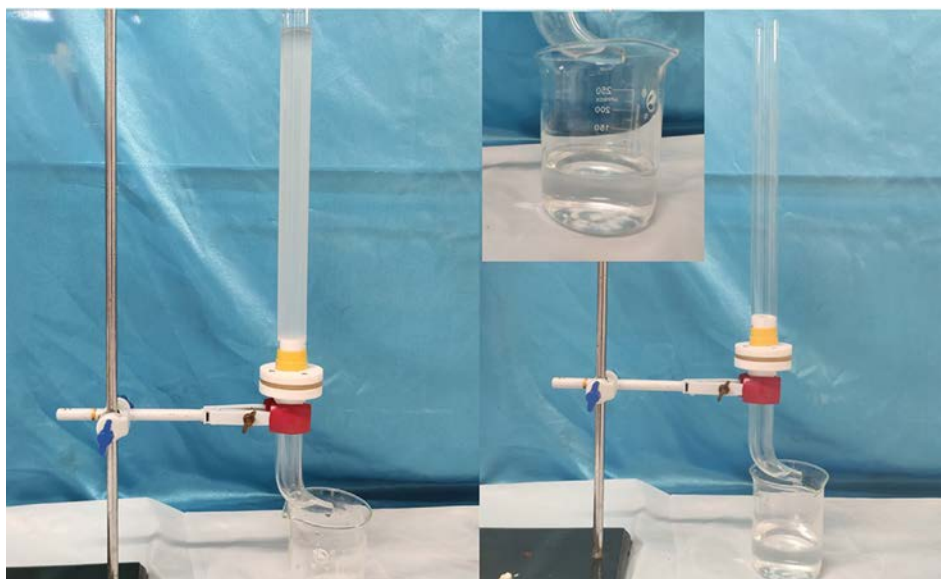
Fig. 7. The apparatus and oil-in-water emulsion separation process. Magnified pictures show clear and transparent water in the beaker after separation.

superhydrophilic and underwater superoleophobic property allowed the penetration of water while oil phase was effectively intercepted on the water layer [50]. In addition, the separation efficiency was utilized to explore the separation performance for oil rejection. Fig. 9a illustrated the separation efficiencies for all tested emulsions. The as-prepared Ti foam exhibited super high separation ability with values more than 99% for kerosene-in-water, petroleum ether-in-water and toluene-in-water, indicating good separation effect for the most of oil-in-water emulsion.

In order to further evaluate the separation performance of modified Ti foams, the permeation fluxes were also investigated. Fig. 9b showed fluxes of different oil/water emulsions, which were all in excess of 900 L m^{-2}h^{-1}, reaching up to 1033, 931, 974, and 1014, 1042, 1018 L m^{-2}h^{-1} for n-hexane, diesel, soybean oil, and petroleum ether, kerosene, toluene, respectively, exhibiting the high fluxes for most of the light oil. It was worth mentioning that distinction of fluxes between different emulsions were not obvious. In fact, the permeate flux of the superhydrophilic Ti foam heavily depends on the oil's density but has little to do with the viscosity, because the oil is the dispersed phase while the water is the continuous phase [51]. The fluxes of higher viscosity oils (diesel and soybean oil) are relatively low, while the lower viscosity oils are on the contrary, such as petroleum ether, toluene, n-hexane. The results of high separation efficiency and permeation flux indicated that the oil-in-water emulsion separation based on the TiO$_2$ nanoarray structures immobilized on the foam was very efficient for application in practical oil/water emulsion treatment.

3.5. Anti-fouling property and self-cleaning performances

As is known to all, the pores of material surface are easy to be blocked by oil during the process of oil/water emulsions separation, which extremely restricts the long-term service life. However, the characteristic of nanostructured TiO$_2$ could endow the Ti foam with anti-fouling performance. Three different tests were applied to investigate the underwater anti-oil-adhesion and self-cleaning behavior. Fig. 10a showed that when pre-wetted Ti foam adhered with machine oil (dyed red) was immersed into water, the oil spontaneously levitated off the foam, leaving clean surface, while the pristine foam was covered by red oil film as a contrast (Fig. S7). Furthermore, the highly viscous machine oil was ejected onto the surface of as-prepared Ti foam underwater with a syringe, and the oil jet immediately bounced up from the surface and immediately floated up to the top of water without any adhesion as shown in Video S3 and Fig. 10b. In the contrast experiments, the pristine one was adhered by large oil droplet. Moreover, the pre-wetted Ti foam was immersed in machine oil/water mixture and lifted up repeatedly, as illustrated in Fig. 10c and Video S4. It was found that there were no red oil droplets on the surface of superhydrophilic foam but the machine oil film covered and polluted the pristine one (Video S5). The three experiments all proved that the fabricated surface possessed excellent anti-fouling and self-cleaning ability underwater, which provided a good strategy for practical application in anti-fouling field.
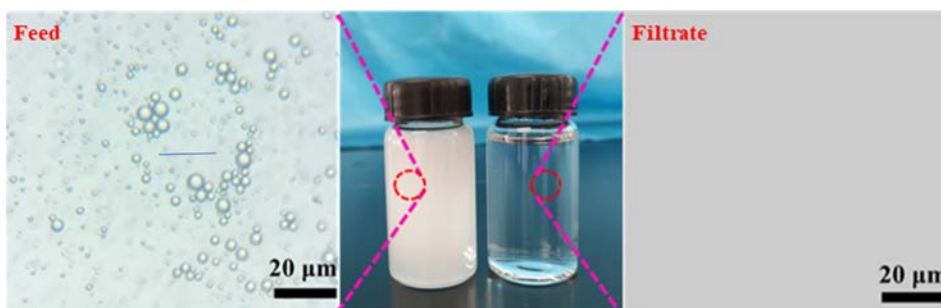
**Fig. 8.** Photograph and micrograph of feed and filtrate.
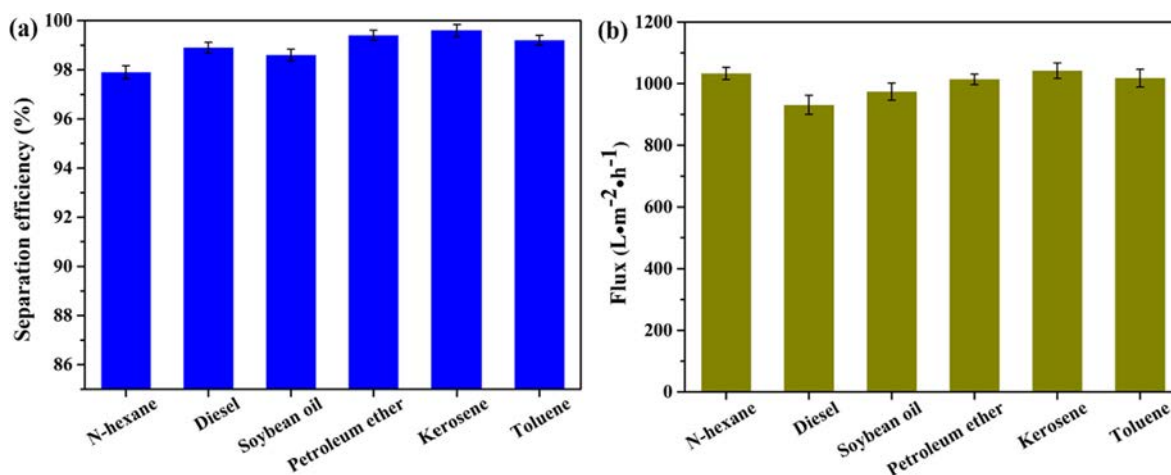
Fig. 9. (a) The separation efficiencies and (b) permeation fluxes for various kinds of oil-in-water emulsions.

3.6. Chemical stability and recyclability of the superhydrophilic Ti foam

The stability and recyclability of materials are the two important factors in the practical oil/water separation. In our work, we conducted oil/water emulsion separation tests to evaluate the recyclability from separation efficiency and underwater OCA. The separation parameters of the nanostructured Ti foam for oil-in-water emulsion (petroleum ether) were recorded per 5 cycles until 50 reuse cycles. Then, the sample was washed with ethanol and deionized water, dried at 60 °C after each oil/water separation test. As shown in Fig. 11a, the superhydrophilic Ti foam maintained high separation efficiency above 99% after alternate cycles. After 50 repeated cycles, the contact angle still remained higher than 155° (Fig. S8). These results demonstrate that our superhydrophilic Ti foam has the superior recyclability performance due to its underwater anti-fouling property.

Moreover, the anti-corrosive property of the chemical stability is of vital importance to the materials used in water purification. Generally, corrosive liquids are sometimes made up of acidic, alkaline or saline

components, or under high or low temperatures. However, the as-prepared Ti foam covering with TiO_2 nanoarray structures possessed a unique anti-corrosive property, which could maintain robust wettability in corrosive environment. Here, the foams were immersed in 1 M HCl, 1 M NaOH, 1 M NaCl aqueous solutions and hot water (80 °C), ice water (0 °C) for 24 h, respectively, following by measuring the separation efficiency of the kerosene-in-water emulsions and underwater OCA of dichloromethane. As illustrated in Fig. 11c, the results showed that the separation efficiency had no obvious alterations than that without corrosive treatments, which were higher than 99%. The results of underwater OCAs all exceeded 160°, performing excellent underwater superoleophobic property. Fig. S9 illustrated that the surface morphology was not broken but kept its intrinsic appearance, which demonstrated that as-prepared Ti foam had excellent stability under a series of corrosive conditions. In addition, the complex composition of wastewater often consisted of organic solvent. Thus, we soaked the as-prepared Ti foam in various organic solvents for 24 h to further evaluate its chemical stability. According to the results illustrated in
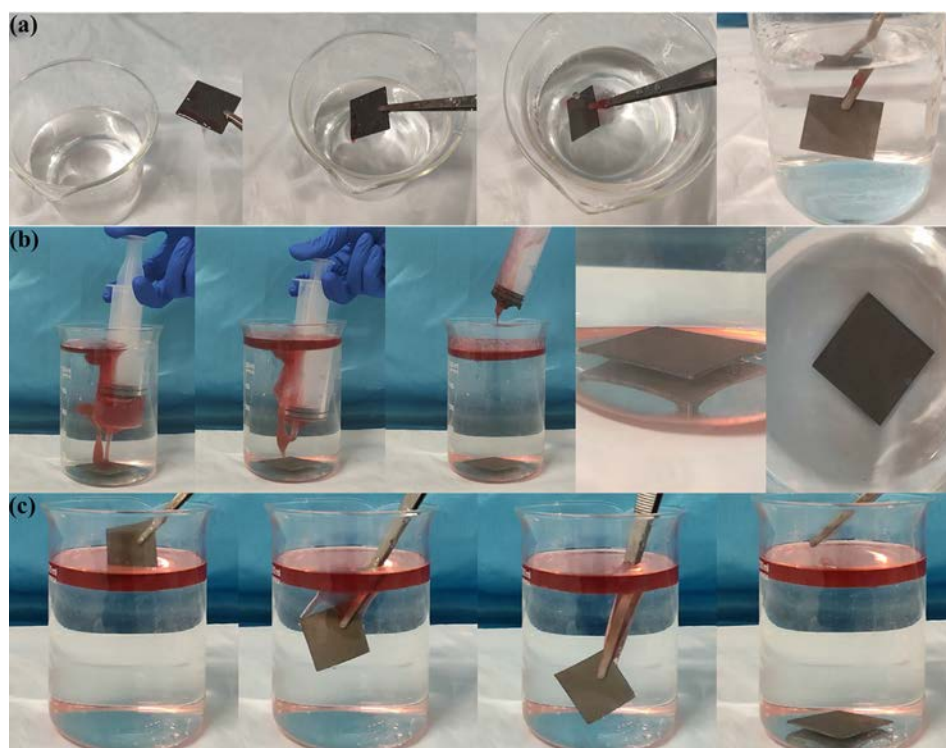
Fig. 10. Underwater anti-fouling and self-cleaning performance of as-prepared foam. (a) The prewetted foam contaminated by machine oil was immersed in water. (b) Machine oil labeled by oil red was injected onto the surface of Ti foam underwater with a syringe. (c) The samples wetted by water were submerged in machine oil-polluted water.
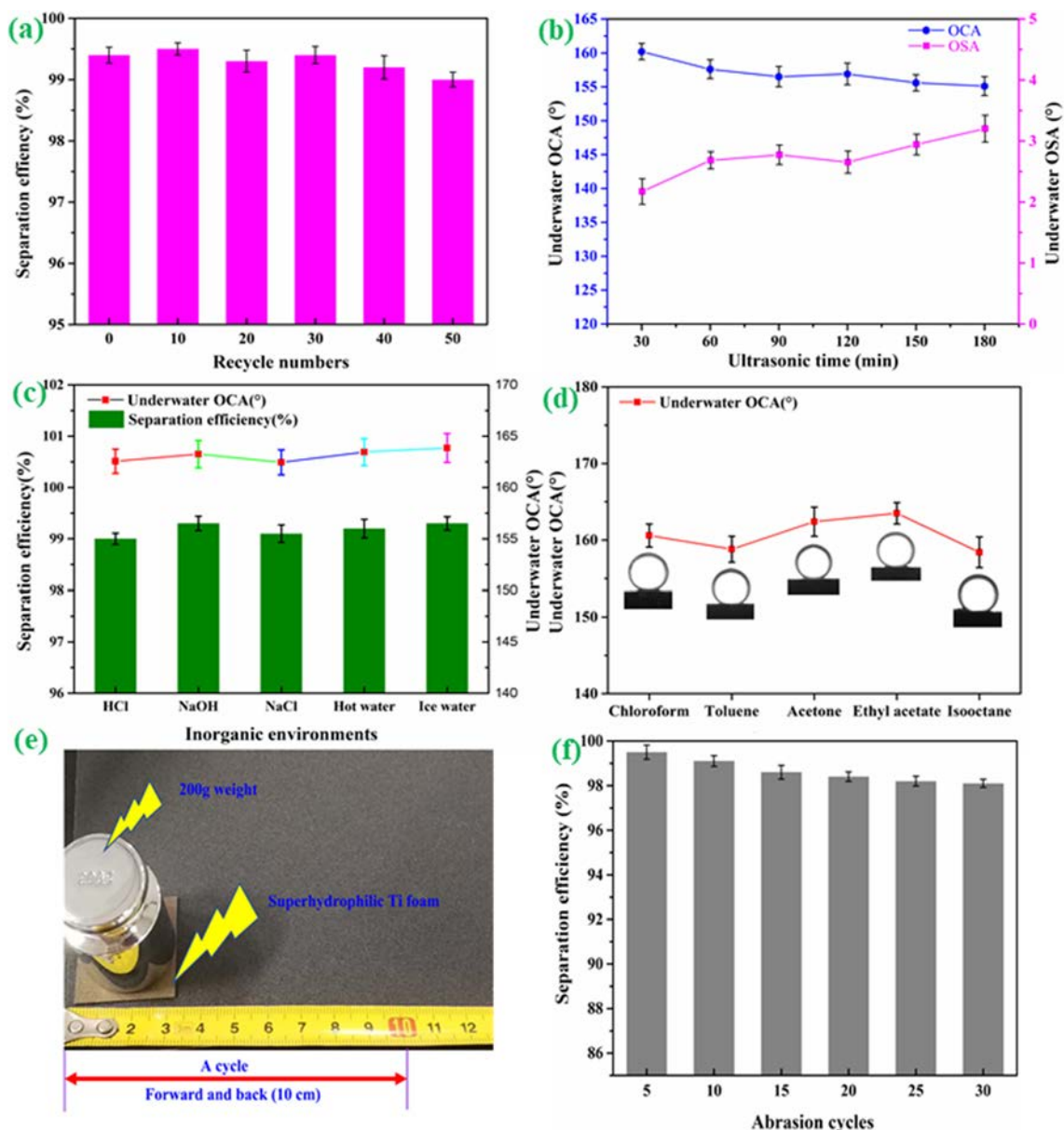
Fig. 11. (a) The petroleum ether-in-water emulsions separation efficiencies of as-prepared Ti foam for repeated use. (b) The underwater OCAs and OSAs with different ultrasonic time. The separation efficiencies and underwater OCA in (c) different inorganic environments and (d) organic solvents. (e) The abrasion tests for as-prepared Ti foam on 400 mesh grit sandpaper and (f) the separation efficiency after different abrasion cycles.

Fig. 11d, underwater OCAs slightly decreased but still remained higher than 155°, and Fig. S10 showed that the surface morphology is without changes. These results indicated that the TiO₂ nanoarray structures could maintain stable not only in corrosive inorganic environments but in organic solvents, which signified that as-prepared Ti foam would have a good practical prospect in oil/water emulsion separation.

3.7. Mechanical stability

The mechanical stability is of critical importance for the surface microstructure which is often damaged by some external mechanical forces such as abrasion and vibration, leading to the loss of separating function of the materials. In fact, it is difficult to avoid the abrasion and vibration in realistic environments. Herein, to demonstrate the mechanical stability of the as-prepared Ti foam, the experiments concerning to the abrasion and the ultrasonic vibration tests were both carried out. The ultrasonic cleaner with power of 1000 W was the source of vibration. Fig. 11b showed the underwater OCAs with

different vibration time. It was clear that the samples could still maintain their underwater superoleophobicity after 3 h vibration. The microstructures of the Ti foam had no apparent variation comparing to original morphology (Fig. S11), manifesting excellent durability against vibration. In addition, the as-prepared Ti foam was placed on 400 mesh sandpaper, meanwhile, a 200 g weight was as an external force to test its anti-abrasion performance. The sample was pulled forward along the direction of ruler for 10 cm, then pushed backward for the same distance as a cycle (Fig. 11e). Importantly, after 30 cycles, the underwater oleophobicity gradually decreased with the increase of cycle times in general, while the underwater OCAs were still higher than 150°, indicating the underwater superoleophobicity still remained, as illustrated in Fig. 11f. Compared to the pristine Ti foam, the appearance of the sample had changed after abrasion cycles (Fig. S12). However, due to the two-dimensional nanoarray structures of vertical growth covering the surface was hierarchical and stably immobilized, only the outermost nanoarray structures of the surface were damaged, but the internal nanoarray structures were not be destroyed, which ensured

that underwater superoleophobicity still kept. Both results of ultrasonic vibration and abrasion tests indicated that the surface components of the foam had robustness and mechanical resistance.

4. Conclusion

In this paper, the superhydrophilic Ti foam with TiO_2 nanoarray structures was fabricated through facile hydrothermal treatment. The growth of anatase TiO_2 on the surface of Ti foam with considerable roughness benefits the superhydrophilicity and underwater superoleophobicity, leading to the rapid water wetting process and ultra-low oil adhesion behaviors. The as-prepared Ti foam realized effective separation of various oil-in-water emulsions with the efficiency higher than 98% only under the action of gravity. In addition, the good underwater anti-fouling and self-cleaning performances realized the feasibility of the foam with TiO_2 nanoarray structures for long-term use. The separation efficiency of kerosene-in-water emulsion still maintained 99% after 50 repeated use. More importantly, the nanoarrays immobilized on the substrate had excellent chemical stability under various harsh conditions including 1 M NaOH, 1 M HCl, 1 M NaCl, hot water, ice water, and organic solvents. Furthermore, the superhydrophilic Ti foam also exhibited robust mechanical property under 30 abrasion cycles and 3 h ultrasonic vibration tests. In summary, it is believed that the Ti foam with good anti-fouling performance, superior chemical stability, robust mechanical property, could make it a competitive candidate for the oily wastewater treatment, microfluidic devices under severe environments.

CRediT authorship contribution statement

Luhong Zhang: Validation, Supervision, Project administration, Funding acquisition, Project administration. **Xiaodong Yang:** Conceptualization, Methodology, Software, Validation, Formal analysis, Investigation, Resources, Data curation, Writing - original draft, Writing - review & editing, Visualization, Supervision, Project administration. **Bin Jiang:** Validation, Supervision, Project administration, Funding acquisition, Project administration. **Yongli Sun:** Validation, Supervision, Project administration, Funding acquisition, Project administration. **Ziqiang Gong:** Software, Validation, Writing - review & editing. **Na Zhang:** Validation, Writing - review & editing, Supervision. **Shuai Hou:** Supervision. **Jingshuai Li:** Supervision. **Na Yang:** Validation, Supervision, Project administration, Funding acquisition, Project administration.

Declaration of Competing Interest

The authors declare that they have no known competing financial interests or personal relationships that could have appeared to influence the work reported in this paper.

Acknowledgments

Appendix A. Supplementary material

Supplementary data to this article can be found online at https://doi.org/10.1016/j.seppur.2020.117437.

References

[1] T. Zhang, Q. Guo, Continuous preparation of polyHIPE monoliths from ionomer-stabilized high internal phase emulsions (HIPEs) for efficient recovery of spilled oils, Chem. Eng. J. 307 (2017) 812–819.

[2] J. Yang, H. Wang, Z. Tao, X. Liu, Z. Wang, R. Yue, Z. Cui, 3D superhydrophobic sponge with a novel compression strategy for effective water-in-oil emulsion separation and its separation mechanism, Chem. Eng. J. 359 (2019) 149–158.

[3] L. Zhang, Z. Gong, B. Jiang, Y. Sun, Z. Chen, X. Gao, N. Yang, Ni-Al layered double hydroxides (LDHs) coated superhydrophobic mesh with flower-like hierarchical structure for oil/water separation, Appl. Surf. Sci. 490 (2019) 145–156.

[4] S.E. Allan, B.W. Smith, K.A. Anderson, Impact of the deepwater horizon oil spill on bioavailable polycyclic aromatic hydrocarbons in Gulf of Mexico coastal waters, Environ. Sci. Technol. 46 (2012) 2033–2039.

[5] B. Wang, W. Liang, Z. Guo, W. Liu, Biomimetic super-lyophobic and super-lyophilic materials applied for oil/water separation: a new strategy beyond nature, Chem. Soc. Rev. 44 (2015) 336–361.

[6] V. Broje, A.A. Keller, Improved mechanical oil spill recovery using an optimized geometry for the skimmer surface, Environ. Sci. Technol. 40 (2006) 7914–7918.

[7] A. Al-Shamrani, A. James, H. Xiao, Separation of oil from water by dissolved air flotation, Colloid Surf. A-Physicochem. Eng. Asp. 209 (2002) 15–26.

[8] H. Gong, B. Yu, F. Dai, Y. Peng, Influence of electric field on water-droplet separated from emulsified oil in a double-field coupling device, Colloid Surf. A-Physicochem. Eng. Asp. 550 (2018) 27–36.

[9] I. Buist, S. Potter, T. Nedwed, J. Mullin, Herding surfactants to contract and thicken oil spills in pack ice for in situ burning, Cold Reg. Sci. Tech. 67 (2011) 3–23.

[10] Z. Grenoble, S. Trabelsi, Mechanisms, performance optimization and new developments in demulsification processes for oil and gas applications, Adv. Colloid Interface Sci. 260 (2018) 32–45.

[11] P. Wang, T. Zhao, R. Bian, G. Wang, H. Liu, Robust superhydrophobic carbon nanotube film with lotus leaf mimetic multiscale hierarchical structures, ACS Nano 11 (2017) 12385–12391.

[12] Y. Zhao, C. Yu, H. Lan, M. Cao, L. Jiang, Improved interfacial floatability of superhydrophobic/superhydrophilic janus sheet inspired by lotus leaf, Adv. Funct. Mater. 27 (2017) 1701466.

[13] N. Cao, B. Yang, A. Barras, S. Szunerits, R. Boukherroub, Polyurethane sponge functionalized with superhydrophobic nanodiamond particles for efficient oil/water separation, Chem. Eng. J. 307 (2017) 319–325.

[14] T. Fan, J. Miao, Z. Li, B. Cheng, Bio-inspired robust superhydrophobic-superoleophilic polyphenylene sulfide membrane for efficient oil/water separation under highly acidic or alkaline conditions, J. Hazard. Mater. 373 (2019) 11–22.

[15] M. Khosravi, S. Azizian, Preparation of superhydrophobic and superoleophilic nanostructured layer on steel mesh for oil-water separation, Sep. Purif. Technol. 172 (2017) 366–373.

[16] J. Wang, A. Wang, Acetylated modification of kapok fiber and application for oil absorption, Fiber. Polym. 14 (2013) 1834–1840.

[17] X. Liu, Y. Wang, Z. Chen, K. Ben, Z. Guan, A self-modification approach toward transparent superhydrophobic glass for rainproofing and superhydrophobic fiberglass mesh for oil water separation, Appl. Surf. Sci. 360 (2016) 789–797.

[18] H.P. Karki, L. Kafle, H.J. Kim, Modification of 3D polyacrylonitrile composite fiber for potential oil-water mixture separation, Sep. Purif. Technol. 229 (2019).

[19] D.-D. La, T.A. Nguyen, S. Lee, J.W. Kim, Y.S. Kim, A stable superhydrophobic and superoleophilic Cu mesh based on copper hydroxide nanoneedle arrays, Appl. Surf. Sci. 257 (2011) 5705–5710.

[20] G. Wang, Z. Zeng, X. Wu, T. Ren, J. Han, Q. Xue, Three-dimensional structured sponge with high oil wettability for the clean-up of oil contaminations and separation of oil–water mixtures, Polym. Chem. 5 (2014) 5942–5948.

[21] J. Lv, Z. Gong, Z. He, J. Yang, Y. Chen, C. Tang, Y. Liu, M. Fan, W.-M. Lau, 3D printing of a mechanically durable superhydrophobic porous membrane for oil–water separation, J. Mater. Chem. A 5 (2017) 12435–12444.

[22] F. Zhang, W.B. Zhang, Z. Shi, D. Wang, J. Jin, L. Jiang, Nanowire-haired inorganic membranes with superhydrophilicity and underwater ultralow adhesive superoleophobicity for high-efficiency oil/water separation, Adv. Mater. 25 (2013) 4192–4198.

[23] J. Wang, J. Wu, F. Han, Eco-friendly and scratch-resistant hybrid coating on mesh for gravity-driven oil/water separation, J. Clean Prod. 241 (2019).

[24] H.P. Karki, L. Kafle, H.J. Kim, Composite membrane of polyacrylonitrile and spent alkaline battery powder for filtration of oil-in-water emulsions, Microporous Mesoporous Mat. 297 (2020).

[25] J. Wang, H. Wang, Easily enlarged and coating-free underwater superoleophobic fabric for oil/water and emulsion separation via a facile NaClO2 treatment, Sep. Purif. Technol. 195 (2018) 358–366.

[26] H.P. Karki, L. Kafle, D.P. Ojha, J.H. Song, H.J. Kim, Cellulose/polyacrylonitrile electrospun composite fiber for effective separation of the surfactant-free oil-in-water mixture under a versatile condition, Sep. Purif. Technol. 210 (2019) 913–919.

[27] Z. Xue, S. Wang, L. Lin, L. Chen, M. Liu, L. Feng, L. Jiang, A novel superhydrophilic and underwater superoleophobic hydrogel-coated mesh for oil/water separation, Adv. Mater. 23 (2011) 4270–4273.

[28] J. Wang, H. Wang, Integrated device based on cauliflower-like nickel hydroxide particles–coated fabrics with inverse wettability for highly efficient oil/hot alkaline water separation, J. Colloid Interface Sci. 534 (2019) 228–238.

[29] J. Ji, H. He, C. Chen, W. Jiang, A. Raza, T.-J. Zhang, S. Yuan, Biomimetic hierarchical TiO2@CuO nanowire arrays-coated copper meshes with superwetting and self-cleaning properties for efficient oil/water separation, ACS Sustain. Chem. Eng. 7 (2018) 2569–2577.

[30] J.S. Chen, Y.L. Tan, C.M. Li, Y.L. Cheah, D. Luan, S. Madhavi, F.Y. Boey, L.A. Archer, X.W. Lou, Constructing hierarchical spheres from large ultrathin anatase TiO2 nanosheets with nearly 100% exposed (001) facets for fast reversible lithium storage, J. Am. Chem. Soc. 132 (2010) 6124–6130.

[31] K. Nakata, A. Fujishima, TiO2 photocatalysis: Design and applications, J. Photochem. Photobiol. C-Photochem. 13 (2012) 169–189.

[32] Q. Chang, J.-E. Zhou, Y. Wang, J. Liang, X. Zhang, S. Cerneaux, X. Wang, Z. Zhu, Y. Dong, Application of ceramic microfiltration membrane modified by nano-TiO2 coating in separation of a stable oil-in-water emulsion, J. Membr. Sci. 456 (2014) 128–133.

[33] M. Tao, L. Xue, F. Liu, L. Jiang, An intelligent superwetting PVDF membrane showing switchable transport performance for oil/water separation, Adv. Mater. 26 (2014) 2943–2948.

[34] J. Li, L. Yan, W. Hu, D. Li, F. Zha, Z. Lei, Facile fabrication of underwater super-oleophobic TiO 2 coated mesh for highly efficient oil/water separation, Colloid Surf. A-Physicochem. Eng. Asp. 489 (2016) 441–446.

[35] S. Li, J. Huang, M. Ge, C. Cao, S. Deng, S. Zhang, G. Chen, K. Zhang, S.S. Al-Deyab, Y. Lai, Robust flower-like TiO2@cotton fabrics with special wettability for effective self-cleaning and versatile oil/water separation, Adv. Mater. Interfaces 2 (2015) 1500220.

[36] D. Li, X. Cheng, X. Yu, Z. Xing, Preparation and characterization of TiO 2 -based nanosheets for photocatalytic degradation of acetylsalicylic acid: Influence of cal-cination temperature, Chem. Eng. J. 279 (2015) 994–1003.

[37] C. Chen, D. Weng, A. Mahmood, S. Chen, J. Wang, Separation mechanism and construction of surfaces with special wettability for oil/water separation, ACS Appl. Mater. Interfaces 11 (2019) 11006–11027.

[38] A. Raza, B. Ding, G. Zainab, M. El-Newehy, S.S. Al-Deyab, J. Yu, In situ cross-linked superwetting nanofibrous membranes for ultrafast oil–water separation, J. Mater. Chem. A 2 (2014) 10137–10145.

[39] C. Wang, X. Zhang, Y. Zhang, Y. Jia, J. Yang, P. Sun, Y. Liu, Hydrothermal growth of layered titanate nanosheet arrays on titanium foil and their topotactic transfor-mation to heterostructured TiO2 photocatalysts, J. Phys. Chem. C 115 (2011) 22276–22285.

[40] D. Li, X. Cheng, X. Yu, Z. Xing, Preparation and characterization of TiO2-based nanosheets for photocatalytic degradation of acetylsalicylic acid: influence of cal-cination temperature, Chem. Eng. J. 279 (2015) 994–1003.

[41] Y. Wu, X. Liu, Z. Yang, L. Gu, Y. Yu, Nitrogen-doped ordered mesoporous anatase TiO2 nanofibers as anode materials for high performance sodium-ion batteries, Small 12 (2016) 3522–3529.

[42] D. Wang, Y. Liu, X. Liu, F. Zhou, W. Liu, Q. Xue, Towards a tunable and switchable water adhesion on a TiO 2 nanotube film with patterned wettability, Chem. Commun. 7018–7020 (2009).

[43] R.P. Antony, T. Mathews, S. Dash, A. Tyagi, Kinetics and physicochemical process of photoinduced hydrophobic↔ superhydrophilic switching of pristine and N-doped TiO2 nanotube arrays, J. Phys. Chem. C 117 (2013) 6851–6860.

[44] F. Shao, J. Sun, L. Gao, S. Yang, J. Luo, Growth of various TiO2 nanostructures for dye-sensitized solar cells, J. Phys. Chem. C 115 (2010) 1819–1823.

[45] W. Wang, H. Lin, J. Li, N. Wang, Formation of titania nanoarrays by hydrothermal reaction and their application in photovoltaic cells, J. Am. Ceram. Soc. 91 (2008) 628–631.

[46] F. Shao, J. Sun, L. Gao, S. Yang, J. Luo, Template-free synthesis of hierarchical TiO2 structures and their application in dye-sensitized solar cells, ACS Appl. Mater. Interfaces 3 (2011) 2148–2153.

[47] X. Peng, A. Chen, Large-scale synthesis and characterization of TiO2-based nanos-tructures on Ti substrates, Adv. Funct. Mater. 16 (2006) 1355–1362.

[48] H. Shi, Y. He, Y. Pan, H. Di, G. Zeng, L. Zhang, C. Zhang, A modified mussel-inspired method to fabricate TiO2 decorated superhydrophilic PVDF membrane for oil/water separation, J. Membr. Sci. 506 (2016) 60–70.

[49] M.A. Gondal, M.S. Sadullah, M.A. Dastageer, G.H. McKinley, D. Panchanathan, K.K. Varanasi, Study of factors governing oil-water separation process using TiO(2) films prepared by spray deposition of nanoparticle dispersions, ACS Appl. Mater. Interfaces 6 (2014) 13422–13429.

[50] S. Yuan, C. Chen, A. Raza, R. Song, T.-J. Zhang, S.O. Pehkonen, B. Liang, Nanostructured TiO2/CuO dual-coated copper meshes with superhydrophilic, un-derwater superoleophobic and self-cleaning properties for highly efficient oil/water separation, Chem. Eng. J. 328 (2017) 497–510.

[51] Z. Cheng, C. Li, H. Lai, Y. Du, H. Liu, M. Liu, K. Sun, L. Jin, N. Zhang, L. Jiang, Recycled superwetting nanostructured copper mesh film: toward bidirectional se-paration of emulsified oil/water mixtures, Adv. Mater. Interfaces 3 (2016).